MOLECULAR PHYSICS, 1996, VOL. 88, NO. 5, 1277–1292

Solomon echoes for spin 7/2 by soft pulse excitation

By SERGEI Z. AGEEV†, PASCAL P. MAN‡ and B. C. SANCTUARY†
† Department of Chemistry, McGill University, Montreal, Qc, Canada H3A 2K6
‡ Laboratorie de Chimie des Surfaces, CNRS URA 1428, Universite Pierre et Marie Curie, 75252 Paris Cedex 05, France

(*Received 11 October 1995; accepted 18 January 1996*)

Solomon echoes are calculated for spin 7/2 in solids taking into account the first-order quadrupolar interaction while the pulses are on. The computation is performed using the algebraic computer program 'MAPLE'. Fifteen echoes are predicted and the amplitude of each echo is calculated. Each satellite transition produces five echoes whereas no echo is detected for the central transition. Among these echoes, six are 'forbidden' which are a result of the refocusing of exclusively multiple quantum coherences which are developed during the first pulse. These echoes cannot be predicted by a calculation based upon 'hard' pulse excitation. The results are valid for any ratio of the quadrupolar coupling to the frequency of the RF field (ω_Q/ω_1).

1. Introduction

Recently, use of computer algebra has made it possible to calculate Solomon [1] and Hahn [2] echoes for soft pulse excitation for higher spin values (e.g. up to 5/2 values). The calculations retain the first-order quadrupolar interaction while the pulse is on. Six Solomon echoes are predicted for spin 5/2. Two of these are the result of refocusing exclusively multiple quantum (MQ) coherences generated by the first pulse. There are no echoes predicted for the central transition. Here we extend this type of calculation to Solomon echoes for spin 7/2. The Solomon echo pulse sequence includes two RF pulses separated by a time delay [3]. This sequence can be applied to static powder samples to generate the spectrum due to satellite transitions which are usually lost in the dead time of the receiver during one pulse experiment. The time delay must be short in comparison to the FID of the central transition in contrast to Hahn echoes [4]. Considering soft pulse excitation allows the prediction of the 15 echoes for spin 7/2. If the first order quadrupolar interaction is ignored, only nine echoes are obtained. These arise from 'hard' pulse excitation and are therefore called allowed echoes. The six others are a result of the refocusing of multiple quantum coherences developed during the first pulse and depend upon the presence of a first order quadrupole. We call these 'forbidden'. Allowed echoes are bell-shaped whereas forbidden ones are the derivatives of bell shaped curves being sine-shaped [5]. The use of the spin echo pulse sequence in NMR is considered in detail in [6]. Solomon echoes arise from the refocusing of off-resonance single and MQ transitions. They are one-dimensional in contrast to MQ MAS NMR [7] where multiple-pulse sequences employing complex phase cyclings are used to refocus on-resonance MQ transitions generating powder spectra due to the central transition. These techniques are essentially two dimensional.

The components of the density matrix necessary to study echoes are calculated here analytically starting from the equilibrium density matrix $\rho(0) = I_z$. From these,

the amplitude of each echo can be determined as the function of both pulse lengths, the time delay and the ratio of ω_Q/ω_1. The results are valid for any ratio of ω_Q/ω_1 and thus the measurement of any echo amplitude as the function of the second pulse length allows the determination of the quadrupolar coupling constant.

2. Theory

The spin echo pulse sequence in question consists of two soft RF pulses of durations t_1 and t_2 applied along the negative x axis with an interpulse delay τ followed by the evolution period t_1. While the pulses are on, the system is described in the rotating frame by the Hamiltonian

$$H = H_Q^{(1)} + H_{RF}, \tag{1}$$

where

$$H_Q^{(1)} = \tfrac{1}{3}\omega_Q[3I_z^2 - I(I+1)],$$

$$\omega_Q = \frac{3e^2qQ}{8I(2I-1)\hbar}(3\cos^2\beta_1 - 1 + \eta\sin^2\beta_1\cos 2\alpha_1),$$

$$H_{RF} = \omega_1 I_x$$

The Euler angles α_1 and β_1 describe the static magnetic field with respect to the quadrupolar principal axis system (QPAS), the RF amplitude ω_1 describes a pulse intensity. Here $H_Q^{(1)}$ is the first order quadrupolar Hamiltonian, ω_Q is the quadrupolar coupling, $e^2qQ/\hbar$ is the quadrupolar coupling constant and η is the asymmetry parameter. During the periods τ and τ_1 the system evolves under the Hamiltonian $H_Q^{(1)}$. The effects of dipole–dipole and second order quadrupolar interactions and relaxation are not considered in the present paper.

The starting point for the calculation of Solomon echoes is the density matrix components related to 1Q coherences, i.e. $\rho_{k\,k-1}(t_1, \tau, t_2, \tau_1)$, where k runs from 5 to 2. The subscripts $k, k-1$ in $\rho_{k\,k-1}(t_1, \tau, t_2, \tau_1)$ denote the kth row and $(k-1)$th column of the density matrix $\rho_{k\,k-1}(t, \tau, t_2, \tau_1)$. The density matrix for the two-pulse experiment with the time delay between the pulses $\rho(t_1, \tau, t_2)$ has been calculated previously [8] taking into account the first order quadrupolar interaction while the pulses are on. The evolution of the density matrix during the acquisition time τ_1 is described by

$$\rho(t_1, \tau, t_2, \tau_1) = \exp(-iH_Q^{(1)}\tau_1)\,\rho(t_1, \tau, t_2)\exp(iH_Q^{(1)}\tau_1). \tag{2}$$

The required components of the density matrix $\rho(t_1, \tau, t_2, \tau_1)$ deduced from equation (2) are

$$\begin{aligned}
\rho_{54}(t_1, \tau, t_2, \tau_1) &= \rho_{54}(t_1, \tau, t_2),\\
\rho_{43}(t_1, \tau, t_2, \tau_1) &= \rho_{43}(t_1, \tau, t_2)\exp(2i\omega_Q\tau_1),\\
\rho_{32}(t_1, \tau, t_2, \tau_1) &= \rho_{32}(t_1, \tau, t_2)\exp(4i\omega_Q\tau_1),\\
\rho_{21}(t_1, \tau, t_2, \tau_1) &= \rho_{21}(t_1, \tau, t_2)\exp(6i\omega_Q\tau_1).
\end{aligned} \tag{3}$$

The intensities of the central line and satellites $F_x^{k\,k-1}$ and $F_y^{k\,k-1}$ can be defined as

$$F_x^{k-1,\,k}(t_1, \tau, t_2, \tau_1) + iF_y^{k-1,\,k}(t_1, \tau, t_2, \tau_1) = \rho_{k\,k-1}(t_1, \tau, t_2, \tau_1). \tag{4}$$

Note that the central line intensity (see equation (3)) does not depend on τ_1 and $F_x^{4,5}(t_1, \tau, t_2, \tau_1) = 0$. In practice, it means that the echo cannot be predicted for the

central transition and the interpulse delay τ must be much shorter than the time of the free induction decay of this transition. This experimental condition is general for all half integer spins [1].

Equations (3) are quite lengthy when developed using 'MAPLE' [9]. Thus only the contributions to the line intensities related to echoes are reported below. For the first inner satellite line (1I-S) the equation for the intensity is given by

$$\begin{aligned}
&F_x^{3,4}(t_1,\tau,t_2,\tau_1)+iF_y^{3,4}(t_1,\tau,t_2,\tau_1)\\
&\quad=\{(I_x^{3,4}+I_x^{3,5})K_1+(I_x^{3,4}-I_x^{3,5})K_2-(I_y^{3,4}+I_y^{3,5})K_3\\
&\quad+(I_y^{3,4}-I_y^{3,5})K_4\}\exp(2i\omega_Q(\tau_1-\tau))\\
&\quad-i\{(I_x^{3,4}+I_x^{3,5})K_3-(I_x^{3,4}-I_x^{3,5})K_4+(I_y^{3,4}+I_y^{3,5})K_1\\
&\quad+(I_y^{3,4}-I_y^{3,5})K_2\}\exp(2i\omega_Q(\tau_1-\tau))\\
&\quad+\{(I_x^{2,3}+I_x^{2,6})K_5+(I_x^{2,3}-I_x^{2,6})K_6-(I_y^{2,3}+I_y^{2,6})K_7\\
&\quad+(I_y^{2,3}-I_y^{2,6})K_8\}\exp(2i\omega_Q(\tau_1-2\tau))\\
&\quad-i\{(I_x^{2,3}+I_x^{2,6})K_7-(I_x^{2,3}-I_x^{2,6})K_8+(I_y^{2,3}+I_y^{2,6})K_5\\
&\quad+(I_y^{2,3}-I_y^{2,6})K_6\}\exp(2i\omega_Q(\tau_1-2\tau))\\
&\quad+\{(I_x^{2,4}+I_x^{2,5})K_9+(I_x^{2,4}-I_x^{2,5})K_{10}-(I_y^{2,4}+I_y^{2,5})K_{11}\\
&\quad+(I_y^{2,4}-I_y^{2,5})K_{12}\}\exp(2i\omega_Q(\tau_1-3\tau))\\
&\quad-i\{(I_x^{2,4}+I_x^{2,5})K_{11}-(I_x^{2,4}-I_x^{2,5})K_{12}+(I_y^{2,4}+I_y^{2,5})K_9\\
&\quad+(I_y^{2,4}-I_y^{2,5})K_{10}\}\exp(2i\omega_Q(\tau_1-3\tau))\\
&\quad+\{(I_x^{1,2}+I_x^{1,7})K_{13}+(I_x^{1,2}-I_x^{1,7})K_{14}-(I_y^{1,2}+I_y^{1,7})K_{15}\\
&\quad+(I_y^{1,2}-I_y^{1,7})K_{16}\}\exp(2i\omega_Q(\tau_1-3\tau))\\
&\quad-i\{(I_x^{1,2}+I_x^{1,7})K_{15}-(I_x^{1,2}-I_x^{1,7})K_{16}+(I_y^{1,2}+I_y^{1,7})K_{13}\\
&\quad+(I_y^{1,2}-I_y^{1,7})K_{14}\}\exp(2i\omega_Q(\tau_i-3\tau))\\
&\quad+\{(I_x^{1,3}+I_x^{1,6})K_{17}+(I_x^{1,3}-I_x^{1,6})K_{18}-(I_y^{1,3}+I_y^{1,6})K_{19}\\
&\quad+(I_y^{1,3}-I_y^{1,6})K_{20}\}\exp(2i\omega_Q(\tau_1-5\tau))\\
&\quad-i\{(I_x^{1,3}+I_x^{1,6})K_{19}-(I_x^{1,3}-I_x^{1,6})K_{20}+(I_y^{1,3}+I_y^{1,6})K_{17}\\
&\quad+(I_y^{1,3}-I_y^{1,6})K_{18}\}\exp(2i\omega_Q(\tau_1-5\tau))\\
&\quad+\{(I_x^{1,4}+I_x^{1,5})K_{21}+(I_x^{1,4}-I_x^{1,5})K_{22}-(I_y^{1,4}+I_y^{1,5})K_{23}\\
&\quad+(I_y^{1,4}-I_y^{1,5})K_{24}\}\exp(2i\omega_Q(\tau_1-6\tau))\\
&\quad-i\{(I_x^{1,4}+I_x^{1,5})K_{23}-(I_x^{1,4}-I_x^{1,5})K_{24}+(I_y^{1,4}+I_y^{1,5})K_{21}\\
&\quad+(I_y^{1,4}-I_y^{1,5})K_{22}\}\exp(2i\omega_Q(\tau_1-6\tau)).
\end{aligned}\tag{5}$$

In this equation, for the sake of compactness, the average brackets, $\langle\ \rangle$, are dropped. Hence each $I_k^{m,n}$ should read $\langle I_k^{m,n}\rangle$ and are functions which depend on the first pulse length t_1 and are given in [8]. The values K_l, $l = 1, \ldots, 24$, are functions of the second pulse length t_2. These are reported in table 1. Note that $K_1 = K_2$ and $K_3 = K_4$.

For the second inner satellite line (2I-S) equation (5) can be used for the line intensity $F_x^{2,3}(t_1,\tau,t_2,\tau_1)+iF_y^{2,3}(t_1,\tau,t_2,\tau_1)$ with the following substitutions, $K_l \rightarrow F_l$, $\tau_1 \rightarrow 2\tau_1$. The F_l values are identical to the K_l's in table 1 except that α and β are given by $\alpha = Y_{1i}Y_{2j}$ and $\beta = Z_{1i}Z_{2j}$. Note that $F_5 = F_6$ and $F_7 = F_8$.

Similarly, for the outer satellite line (O-S), $F_x^{1,2}(t_1,\tau,t_2,\tau_1)+iF_y^{1,2}(t_1,\tau,t_2,\tau_1)$, one can use equation (5) changing $K_l \rightarrow G_l$, $\tau_1 \rightarrow 3\tau_1$, and substituting $\alpha = X_{1i}Z_{2j}$ and $\beta = Y_{1i}T_{2j}$ for the values in table 1. Note that in this case $G_{13} = G_{14}$ and $G_{15} = G_{16}$.

Table 1. Values K_l with $\alpha = Z_{1i}X_{2j}$ and $\beta = T_{1i}Y_{2j}$. Summation convention, $i, j = 1, 4$, is used. The X's, Y's, Z's, T's and ω_{ij}'s are reported in [10].

$K_1 = \beta Z_{1i}X_{2j}\cos\omega_{ij}t_2$	$K_2 = \alpha T_{1i}Y_{2j}\cos\omega_{ij}t_2$
$K_3 = \beta Z_{1i}X_{2j}\sin\omega_{ij}t_2$	$K_4 = \alpha T_{1j}Y_{2j}\sin\omega_{ij}t_2$
$K_5 = \beta Y_{1i}Y_{2j}\cos\omega_{ij}t_2$	$K_6 = \alpha Z_{1i}Z_{2j}\cos\omega_{ij}t_2$
$K_7 = \beta Y_{1i}Y_{2j}\sin\omega_{ij}t_2$	$K_8 = \alpha Z_{1i}Z_{2j}\sin\omega_{ij}t_2$
$K_9 = \beta Y_{1i}X_{2j}\cos\omega_{ij}t_2$	$K_{10} = \alpha T_{1i}Z_{2j}\cos\omega_{ij}t_2$
$K_{11} = \beta Y_{1i}X_{2j}\sin\omega_{ij}t_2$	$K_{12} = \alpha T_{1i}Z_{2j}\sin\omega_{ij}t_2$
$K_{13} = \beta X_{1i}Z_{2j}\cos\omega_{ij}t_2$	$K_{14} = \alpha Y_{1i}T_{2j}\cos\omega_{ij}t_2$
$K_{15} = \beta X_{1i}Z_{2j}\sin\omega_{ij}t_2$	$K_{16} = \alpha Y_{1i}T_{2j}\sin\omega_{ij}t_2$
$K_{17} = \beta X_{1i}Y_{2j}\cos\omega_{ij}t_2$	$K_{18} = \alpha Z_{1i}T_{2j}\cos\omega_{ij}t_2$
$K_{19} = \beta X_{1i}Y_{2j}\sin\omega_{ij}t_2$	$K_{20} = \alpha Z_{1i}T_{2j}\sin\omega_{ij}t_2$
$K_{21} = \beta X_{1i}X_{2j}\cos\omega_{ij}t_2$	$K_{22} = \alpha T_{1i}T_{2j}\cos\omega_{ij}t_2$
$K_{23} = \beta X_{1i}X_{2j}\sin\omega_{ij}t_2$	$K_{24} = \alpha T_{1i}T_{2j}\sin\omega_{ij}t_2$

The echoes corresponding to $F_x^{k-1,k}(t_1, \tau, t_2, \tau_1) + iF_y^{k-1,k}(t_1, \tau, t_2, \tau_1)$ with $k = 3$ are seen to be twice as broad as those with $k = 4$, whereas echoes with $k = 2$ are three-times as broad as those with $k = 4$. This is seen from equation (3).

In quadrature detection mode, one can observe 15 echoes in both channels. The echoes described by $F_x^{3,4}(t_1, \tau, t_2, \tau_1) + iF_y^{3,4}(t_1, \tau, t_2, \tau_1)$ are located at $\tau_1 = \tau$, $\tau_1 = 2\tau$, $\tau_1 = 3\tau$, $\tau_1 = 5\tau$ and $\tau_1 = 6\tau$. The echoes which correspond to $F_x^{2,3}(t_1, \tau, t_2, \tau_1) + iF_y^{2,3}(t_1, \tau, t_2, \tau_1)$ are detected at $\tau_1 = \tau/2$, $\tau_1 = \tau$, $\tau_1 = 3\tau/2$, $\tau_1 = 5\tau/2$ and $\tau_1 = 3\tau$. For the outer satellite line with the line intensities $F_x^{1,2}(t_1, \tau, t_2, \tau_1) + iF_y^{1,2}(t_1, \tau, t_2, \tau_1)$, the echoes are at $\tau_1 = \tau/3$, $\tau_1 = 2\tau/3$, $\tau_1 = \tau$, $\tau_1 = 5\tau/3$ and $\tau_1 = 2\tau$. These echoes are the result of the refocusing of off-resonance coherences developed during the first pulse. Each echo includes two contributions responsible for the shape of the echo. The first one is related to the sine function which gives sine type shape echoes, while the second one is related to the cosine function which gives symmetrical bell shaped echoes. The contributions of the sine type are equal to zero at the positions where bell shaped contributions have maximums and thus the maximums of bell type echoes are not modified by sine-type echoes. However, the shapes of the echoes can vary ranging from a symmetrical bell to a sine type shape depending on the experimental conditions.

The equations for the amplitude of each echo are given below. As a rule [1], measuring the amplitudes of the echoes as the functions of the second pulse length allows the determination of the quadrupolar coupling ω_Q for single crystals or quadrupolar coupling constant $e^2qQ/\hbar$ and asymmetry parameter η for powders.

3. Summary of echoes

(1) The amplitudes of the first echo located at $\tau_1 = \tau/3$ are given by

$$E_y^{1,2}(t_1, t_2, \tau_1 = \tau/3) = -((I_x^{3,4} + I_x^{3,5})G_3 - (I_x^{3,4} - I_x^{3,5})G_4 + (I_y^{3,4} + I_y^{3,5})G_1 + (I_y^{3,4} - I_y^{3,5})G_2) \quad (6)$$

and

$$E_x^{1,2}(t_1, t_2, \tau_1 = \tau/3) = (I_x^{3,4} + I_x^{3,5})G_1 + (I_x^{3,4} - I_x^{3,5})G_2 - (I_y^{3,4} + I_y^{3,5})G_3 + (I_y^{3,4} - I_y^{3,5})G_4. \quad (7)$$

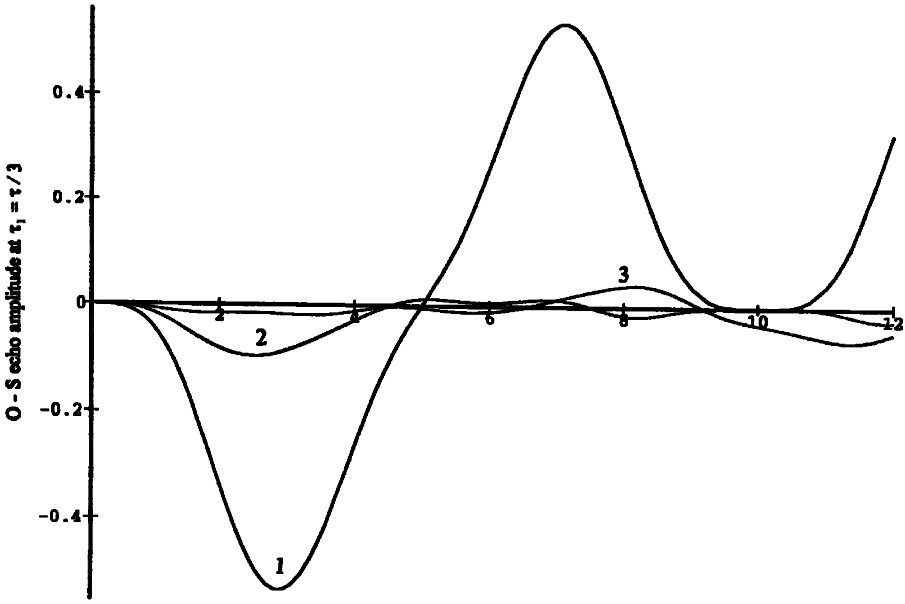

Figure 1. Spin echo amplitude $E_y^{1,2}(t_1, t_2, \tau_1 = \tau/3)$, $\omega_1/2\pi = 50$ kHz, as a function of the second pulse length t_2(μs) for (1) $t_1 = 5$ μs, $\omega_Q/2\pi = 0$ kHz; (2) $t_1 = 3$ μs, $\omega_Q/2\pi = 50$ kHz; (3) spin echo amplitude $E_x^{1,2}(t_1, t_2, \tau_1 = \tau/3)$, $\omega_1/2\pi = 50$ kHz, for $t_1 = 3$ μs, $\omega_Q/2\pi = 50$ kHz.

Figure 1 shows graphs of $E_x^{1,2}(t_1, t_2, \tau_1 = \tau/3)$ and $E_y^{1,2}(t_1, t_2, \tau_1 = \tau/3)$ as functions of the second pulse length.

(2) The amplitudes of the second echo located at $\tau_1 = \tau/2$ are given by

$$E_y^{2,3}(t_1, t_2, \tau_1 = \tau/2) = -((I_x^{3,4} + I_x^{3,5})F_3 - (I_x^{3,4} - I_x^{3,5})F_4 + (I_y^{3,4} + I_y^{3,5})F_1 + (I_y^{3,5} - I_y^{3,5})F_2) \quad (8)$$

and

$$E_x^{2,3}(t_1, t_2, \tau_1 = \tau/2) = (I_x^{3,4} + I_x^{3,5})F_1 + (I_x^{3,4} - I_x^{3,5})F_2 - (I_y^{3,4} + I_y^{3,5})F_3 + (I_y^{3,4} - I_y^{3,5})F_4. \quad (9)$$

Figure 2 shows graphs of $E_x^{2,3}(t_1, t_2, \tau_1 = \tau/2)$ and $E_y^{2,3}(t_1, t_2, \tau_1 = \tau/2)$ as functions of the second pulse length.

These two echoes are the result of refocusing the 1I-S ($3 \leftrightarrow 4$) and 2Q ($3 \leftrightarrow 5$) coherences.

(3) The amplitudes of the third echo located at $\tau_1 = 2\tau/3$ are given by

$$E_y^{1,2}(t_1, t_2, \tau_1 = 2\tau/3) = -((I_x^{2,3} + I_x^{2,6})G_7 - (I_x^{2,3} - I_x^{2,6})G_8 + (I_y^{2,3} + I_y^{2,6})G_5 + (I_y^{2,3} - I_y^{2,6})G_6) \quad (10)$$

and

$$E_x^{1,2}(t_1, t_2, \tau_1 = 2\tau/3) = (I_x^{2,3} + I_x^{2,6})G_5 + (I_x^{2,3} - I_x^{2,6})G_6 - (I_y^{2,3} + I_y^{2,6})G_7 + (I_y^{2,3} - I_y^{2,6})G_8 \quad (11)$$

The echo is the result of refocusing the 2I-S ($2 \leftrightarrow 3$) and 4Q ($2 \leftrightarrow 6$) coherences.

Figure 3 shows graphs of $E_x^{1,2}(t_1, t_2, \tau_1 = 2\tau/3)$ and $E_y^{1,2}(t_1, t_2, \tau_1 = 2\tau/3)$ as functions of the second pulse length.

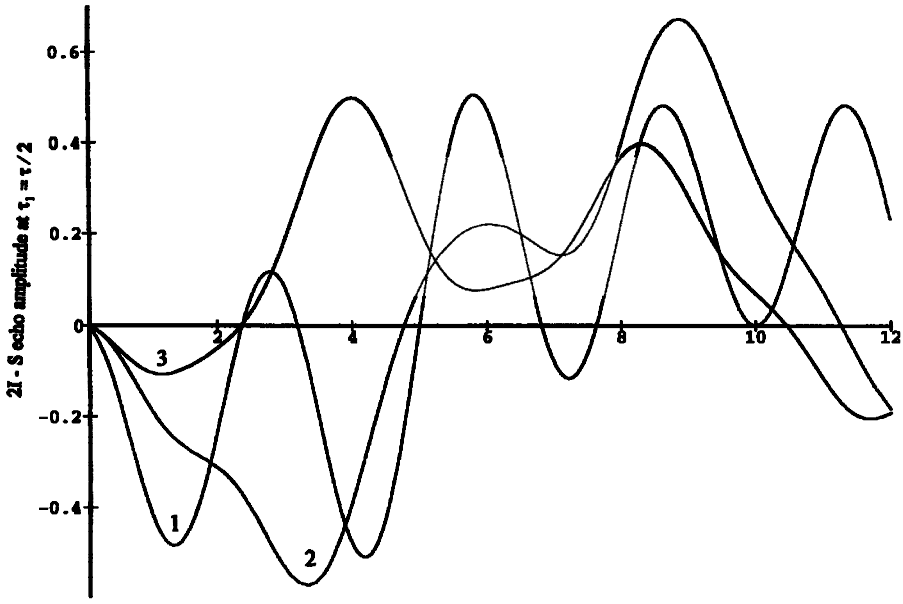

Figure 2. Spin echo amplitude $E_y^{2,3}(t_1, t_2, \tau_1 = \tau/2)$, $\omega_1/2\pi = 50$ kHz, as a function of the second pulse length t_2 (μs) for (1) $t_1 = 5$ μs, $\omega_Q/2\pi = 0$ kHz; (2) $t_1 = 3$ μs, $\omega_Q/2\pi = 50$ kHz; (3) spin echo amplitude $E_x^{2,3}(t_1, t_2, \tau_1 = \tau/2)$, $\omega_1/2\pi = 50$ kHz, for $t_1 = 3$ μs, $\omega_Q/2\pi = 50$ kHz.

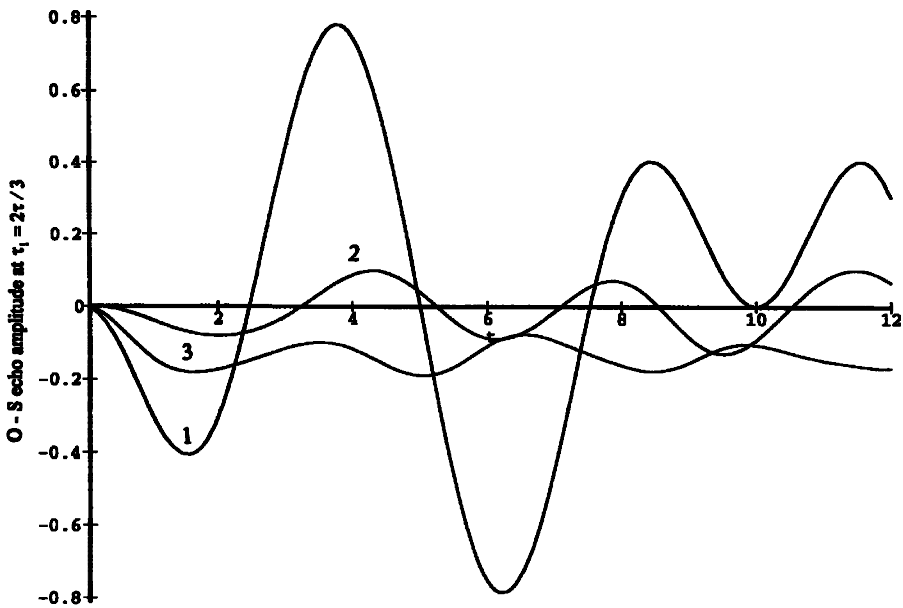

Figure 3. Spin echo amplitude $E_y^{1,2}(t_1, t_2, \tau_1 = 2\tau/3)$, $\omega_1/2\pi = 50$ kHz, as a function of the second pulse length t_2 (μs) for (1) $t_1 = 5$ μs, $\omega_Q/2\pi = 0$ kHz; (2) $t_1 = 3$ μs, $\omega_Q/2\pi = 50$ kHz; (3) spin echo amplitude $E_x^{1,2}(t_1, t_2, \tau_1 = 2\tau/3)$, $\omega_1/2\pi = 50$ kHz, for $t_1 = 3$ μs, $\omega_Q/2\pi = 50$ kHz.

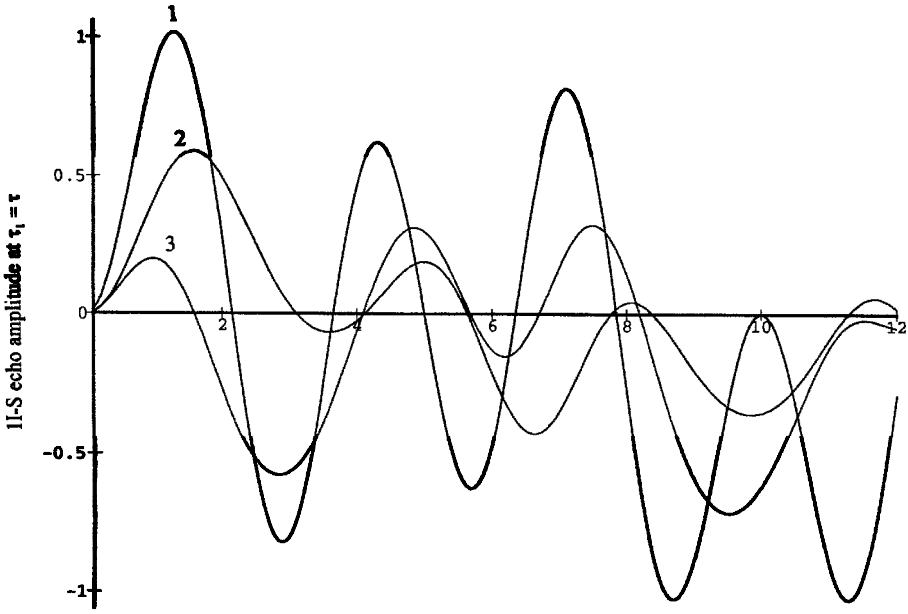

Figure 4. Spin echo amplitude $E_y^{3,4}(t_1, t_2, \tau_1 = \tau)$, $\omega_1/2\pi = 50$ kHz, as a function of the second pulse length t_2 (μs) for (1) $t_1 = 5$ μs, $\omega_Q/2\pi = 0$ kHz; (2) $t_1 = 3$ μs, $\omega_Q/2\pi = 50$ kHz; (3) spin echo amplitude $E_x^{3,4}(t_1, t_2, \tau_1 = \tau)$, $\omega_1/2\pi = 50$ kHz, for $t_1 = 3$ μs, $\omega_Q/2\pi = 50$ kHz.

(4) At the time $\tau_1 = \tau$, three overlapping echoes of different widths are detected. The amplitudes of the echo related to the 1I-S are given by

$$E_y^{3,4}(t_1, t_2, \tau_1 = \tau) = -2(I_x^{3,5}K_3 + I_y^{3,4}K_1) \tag{12}$$

and

$$E_x^{3,4}(t_1, t_2, \tau_1 = \tau) = 2(I_x^{3,4}K_1 - I_y^{3,5}K_3). \tag{13}$$

This echo is the result of refocusing the 1I-S ($3 \leftrightarrow 4$) and 2Q ($3 \leftrightarrow 5$) coherences.

Figure 4 shows graphs of $E_x^{3,4}(t_1, t_2, \tau_1 = \tau)$ and $E_y^{3,4}(t_1, t_2, \tau_1 = \tau)$ as functions of the second pulse length.

(5) The amplitudes of the echo related to the 2I-S are given by

$$E_y^{2,3}(t_1, t_2, \tau_1 = \tau) = -2(I_x^{2,6}F_7 + I_y^{2,3}F_5) \tag{14}$$

and

$$E_x^{2,3}(t_1, t_2, \tau_1 = \tau) = 2(I_x^{2,3}F_5 - I_y^{2,6}F_7). \tag{15}$$

This echo is the result of refocusing the 2I-S ($2 \leftrightarrow 3$) and 4Q ($2 \leftrightarrow 6$) coherences.

Figure 5 shows graphs of $E_x^{2,3}(t_1, t_2, \tau_1 = \tau)$ and $E_y^{2,3}(t_1, t_2, \tau_1 = \tau)$ as functions of the second pulse length.

(6) The amplitudes of the echo related to the O-S are

$$\begin{aligned} E_y^{1,2}(t_1, t_2, \tau_1 = \tau) &= -((I_x^{2,4} + I_x^{2,5})G_{11} - (I_x^{2,4} - I_x^{2,5})G_{12} + (I_y^{2,4} + I_y^{2,5})G_9 \\ &\quad + (I_y^{2,4} - I_y^{2,5})G_{10}) - I_x^{1,7}G_{15} - I_y^{1,2}G_{13} \end{aligned} \tag{16}$$

and

$$\begin{aligned} E_x^{1,2}(t_1, t_2, \tau_1 = \tau) &= (I_x^{2,4} + I_x^{2,5})G_9 + (I_x^{2,4} - I_x^{2,5})G_{10} - (I_y^{2,4} + I_y^{2,5})G_{11} \\ &\quad + (I_y^{2,4} - I_y^{2,5})G_{12} + I_x^{1,2}G_{13} - I_y^{1,7}G_{15}. \end{aligned} \tag{17}$$

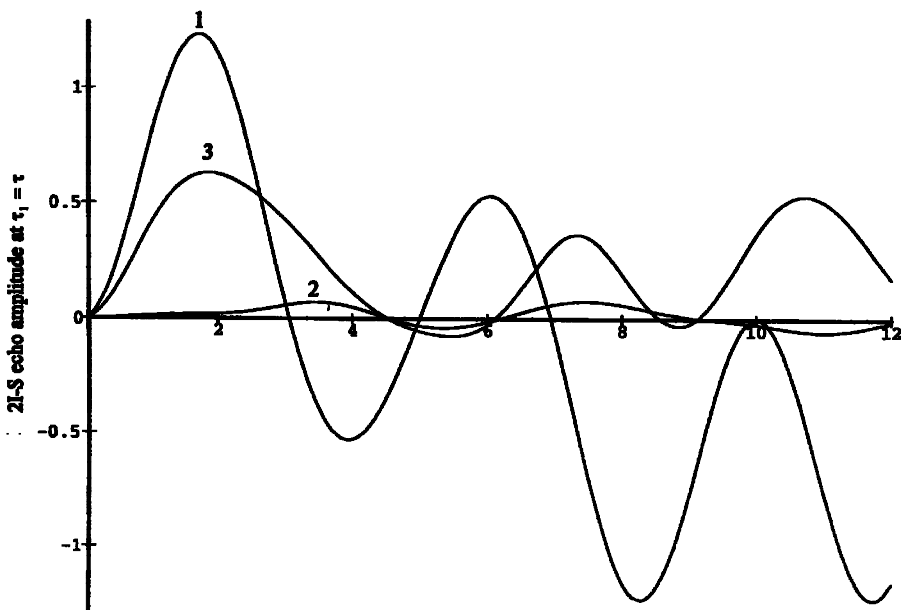

Figure 5. Spin echo amplitude $E_y^{2,3}(t_1, t_2, \tau_1 = \tau)$, $\omega_1/2\pi = 50$ kHz, as a function of the second pulse length t_2 (μs) for (1) $t_1 = 5$ μs, $\omega_Q/2\pi = 0$ kHz; (2) $t_1 = 3$ μs, $\omega_Q/2\pi = 50$ kHz; (3) spin echo amplitude $E_x^{2,3}(t_1, t_2, \tau_1 = \tau)$, $\omega_1/2\pi = 50$ kHz, for $t_1 = 3$ μs, $\omega_Q/2\pi = 50$ kHz.

This echo is the result of refocusing the O-S ($1 \leftrightarrow 2$), 6Q ($1 \leftrightarrow 7$), 2Q ($2 \leftrightarrow 4$) and 3Q ($2 \leftrightarrow 5$) coherences.

Figure 6 shows graphs of $E_x^{1,2}(t_1, t_2, \tau_1 = \tau)$ and $E_y^{1,2}(t_1, t_2, \tau_1 = \tau)$ as functions of the second pulse length.

(7) The amplitudes of the seventh echo located at $\tau_1 = 3\tau/2$ are given by

$$\begin{aligned} E_y^{2,3}(t_1, t_2, \tau_1 = 3\tau/2) \\ = -((I_x^{2,4} + I_x^{2,5})F_{11} - (I_x^{2,4} - I_x^{2,5})F_{12} + (I_y^{2,4} + I_y^{2,5})F_9 + (I_y^{2,4} - I_y^{2,5})F_{10}) \\ -((I_x^{1,2} + I_x^{1,7})F_{15} - (I_x^{1,2} + I_x^{1,7})F_{16} + (I_y^{1,2} + I_y^{1,7})F_{13} + (I_y^{1,2} - I_y^{1,7})F_{14}) \end{aligned} \quad (18)$$

and

$$\begin{aligned} E_x^{2,3}(t_1, t_2, \tau_1 = 3\tau/2) \\ = (I_x^{2,4} + I_x^{2,5})F_9 + (I_x^{2,4} - I_x^{2,5})F_{10} - (I_y^{2,4} + I_y^{2,5})F_{11} + (I_y^{2,4} - I_y^{2,5})F_{12} \\ + (I_x^{1,2} + I_x^{1,7})F_{13} + (I_x^{1,2} + I_x^{1,7})F_{14} - (I_y^{1,2} + I_y^{1,7})F_{15} + (I_y^{1,2} - I_y^{1,7})F_{16} \end{aligned} \quad (19)$$

This echo is the result of refocusing the O-S ($1 \leftrightarrow 2$), 2Q ($2 \leftrightarrow 4$), 3Q ($2 \leftrightarrow 5$) and 6Q ($1 \leftrightarrow 7$) coherences.

Figure 7 shows graphs of $E_x^{2,3}(t_1, t_2, \tau_1 = 3\tau/2)$ and $E_y^{2,3}(t_1, t_2, \tau_1 = 3\tau/2)$ as functions of the second pulse length.

(8) The amplitudes of the eighth echo located at $\tau_1 = 5\tau/3$ are given by

$$\begin{aligned} E_y^{1,2}(t_1, t_2, \tau_1 = 5\tau/3) \\ = -((I_x^{1,3} + I_x^{1,6})G_{19} - (I_x^{1,3} - I_x^{1,6})G_{20} + (I_y^{1,3} + I_y^{1,6})G_{17} + (I_y^{1,3} - I_y^{1,6})G_{18}) \end{aligned} \quad (20)$$

and

$$\begin{aligned} E_x^{1,2}(t_1, t_2, \tau_1 = 5\tau/3) \\ = (I_x^{1,3} + I_x^{1,6})G_{17} + (I_x^{1,3} - I_x^{1,6})G_{18} - (I_y^{1,3} + I_y^{1,6})G_{19} + (I_y^{1,3} - I_y^{1,6})G_{20} \end{aligned} \quad (21)$$

This echo is the result of refocusing the 2Q ($1 \leftrightarrow 3$) and 5Q ($1 \leftrightarrow 6$) coherences.

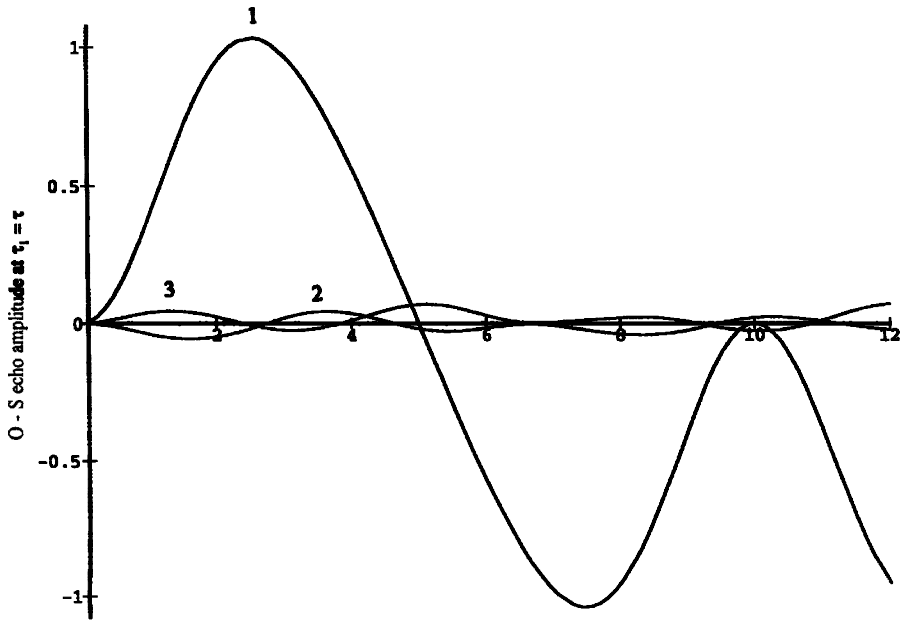

Figure 6. Spin echo amplitude $E_y^{1,2}(t_1, t_2, \tau_1 = \tau)$, $\omega_1/2\pi = 50$ kHz, as a function of the second pulse length t_2 (μs) for (1) $t_1 = 5$ μs, $\omega_Q/2\pi = 0$ kHz; (2) $t_1 = 3$ μs, $\omega_Q/2\pi = 50$ kHz; (3) spin echo amplitude $E_x^{1,2}(t_1, t_2, \tau_1 = \tau)$, $\omega_1/2\pi = 50$ kHz, for $t_1 = 3$ μs, $\omega_Q/2\pi = 50$ kHz.

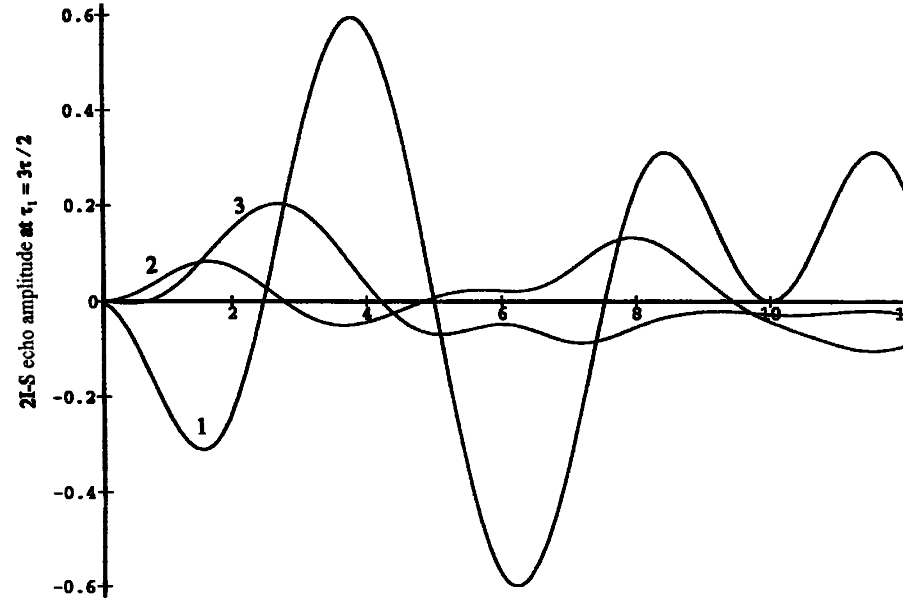

Figure 7. Spin echo amplitude $E_y^{2,3}(t_1, t_2, \tau_1 = 3\tau/2)$, $\omega_1/2\pi = 50$ kHz, as a function of the second pulse length t_2 (μs) for (1) $t_1 = 5$ μs, $\omega_Q/2\pi = 0$ kHz; (2) $t_1 = 3$ μs, $\omega_Q/2\pi = 50$ kHz; (3) spin echo amplitude $E_x^{2,3}(t_1, t_2, \tau_1 = 3\tau/2)$, $\omega_1/2\pi = 50$ kHz, for $t_1 = 3$ μs, $\omega_Q/2\pi = 50$ kHz.

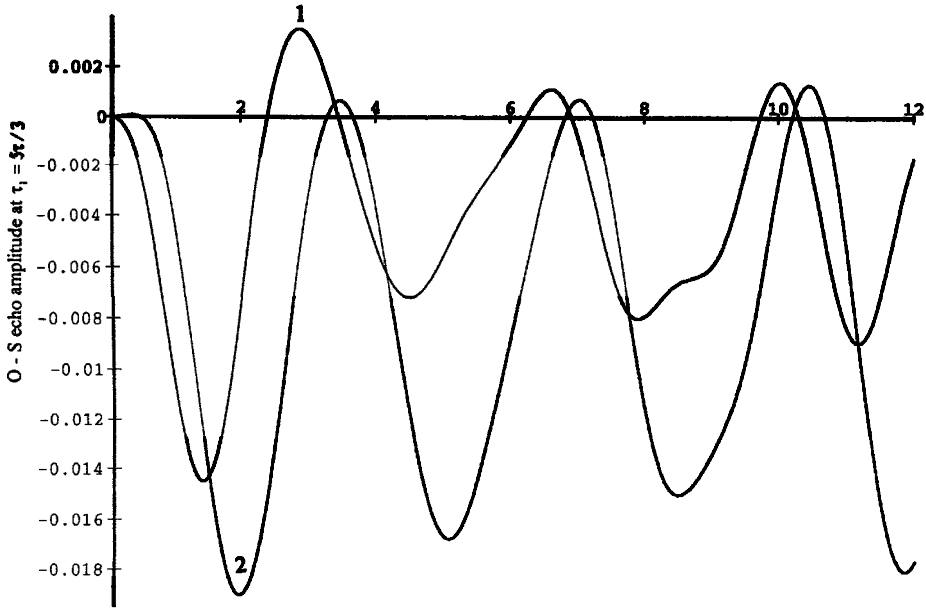

Figure 8. Spin echo amplitude $E_y^{1,2}(t_1, t_2, \tau_1 = 5\tau/3)$, $\omega_1/2\pi = 50$ kHz, as a function of the second pulse length t_2 (μs) for (1) $t_1 = 3$ μs, $\omega_Q/2\pi = 50$ kHz; (2) spin echo amplitude $E_x^{1,2}(t_1, t_2, \tau_1 = 5\tau/3)$, $\omega_1/2\pi = 50$ kHz, for $t_1 = 3$ μs, $\omega_Q/2\pi = 50$ kHz.

Figure 8 shows graphs of $E_x^{1,2}(t_1, t_2, \tau_1 = 5\tau/3)$ and $E_y^{1,2}(t_1, t_2, \tau_1 = 5\tau/3)$ as functions of the second pulse length.

(9) At the time $\tau_1 = 2\tau$, two overlapping echoes of different widths are detected. The amplitudes of the echo related to the 1I-S are given by

$$E_y^{3,4}(t_1, t_2, \tau_1 = 2\tau) = -((I_x^{2,3} + I_x^{2,6})K_7 - (I_x^{2,3} - I_x^{2,6})K_8 + (I_y^{2,3} + I_y^{2,6})K_5 + (I_y^{2,3} - I_y^{2,6})K_6) \quad (22)$$

and

$$E_x^{3,4}(t_1, t_2, \tau_1 = 2\tau) = (I_x^{2,3} + I_x^{2,6})K_5 + (I_x^{2,3} - I_x^{2,6})K_6 - (I_y^{2,3} + I_y^{2,6})K_7 + (I_y^{2,3} - I_y^{2,6})K_8 \quad (23)$$

This echo is the result of refocusing the 2I-S ($2 \leftrightarrow 3$) and 4Q ($2 \leftrightarrow 6$) coherences.

Figure 9 shows graphs of $E_x^{3,4}(t_1, t_2, \tau_1 = 2\tau)$ and $E_y^{3,4}(t_1, t_2, \tau_1 = 2\tau)$ as functions of the second pulse length.

(10) The amplitudes of the echo related to the O-S are given by

$$E_y^{1,2}(t_1, t_2, \tau_1 = 2\tau) = -((I_x^{1,4} + I_x^{1,5})G_{23} - (I_x^{1,4} - I_x^{1,5})G_{24} + (I_y^{1,4} + I_y^{1,5})G_{21} + (I_y^{1,4} - I_y^{1,5})G_{22}) \quad (24)$$

and

$$E_x^{1,2}(t_1, t_2, \tau_1 = 2\tau) = (I_x^{1,4} + I_x^{1,5})G_{21} + (I_x^{1,4} - I_x^{1,5})G_{22} - (I_y^{1,4} + I_y^{1,5})G_{23} + (I_y^{1,4} - I_y^{1,5})G_{24}. \quad (25)$$

This echo is the result of refocusing the 3Q ($1 \leftrightarrow 4$) and 4Q ($1 \leftrightarrow 5$) coherences.

Figure 10 shows graphs of $E_x^{1,2}(t_1, t_2, \tau_1 = 2\tau)$ and $E_y^{1,2}(t_1, t_2, \tau_1 = 2\tau)$ as functions of the second pulse length.

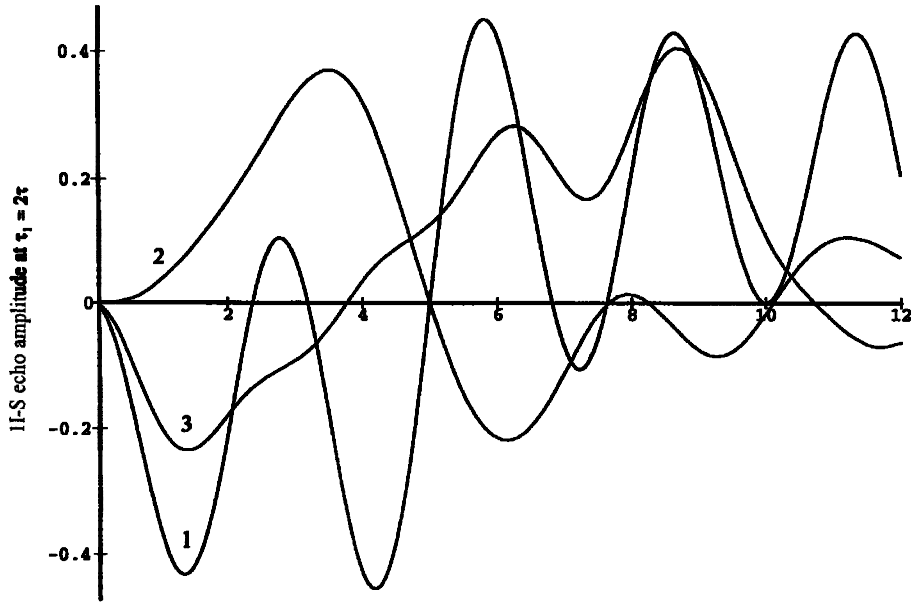

Figure 9. Spin echo amplitude $E_y^{3,4}(t_1, t_2, \tau_1 = 2\tau)$, $\omega_1/2\pi = 50$ kHz, as a function of the second pulse length t_2 (μs) for (1) $t_1 = 5$ μs, $\omega_Q/2\pi = 0$ kHz; (2) $t_1 = 3$ μs, $\omega_Q/2\pi = 50$ kHz; (3) spin echo amplitude $E_x^{3,4}(t_1, t_2, \tau_1 = 2\tau)$, $\omega_1/2\pi = 50$ kHz, for $t_1 = 3$ μs, $\omega_Q/2\pi = 50$ kHz.

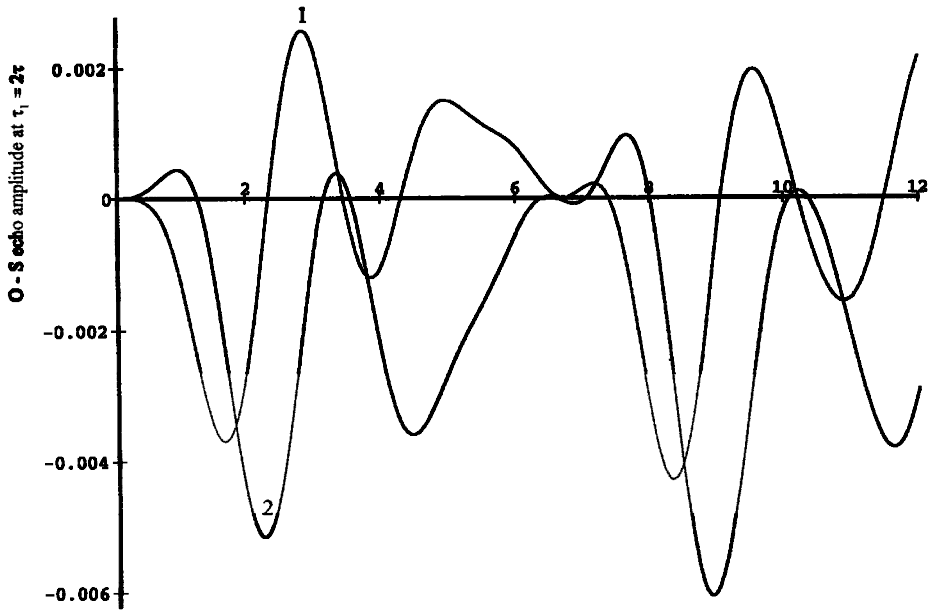

Figure 10. Spin echo amplitude $E_y^{1,2}(t_1, t_2, \tau_1 = 2\tau)$, $\omega_1/2\pi = 50$ kHz, as a function of the second pulse length t_2 (μs) for (1) $t_1 = 3$ μs, $\omega_Q/2\pi = 50$ kHz; (2) spin echo amplitude $E_x^{1,2}(t_1, t_2, \tau_1 = 2\tau)$, $\omega_1/2\pi = 50$ kHz, for $t_1 = 3$ μs, $\omega_Q/2\pi = 50$ kHz.

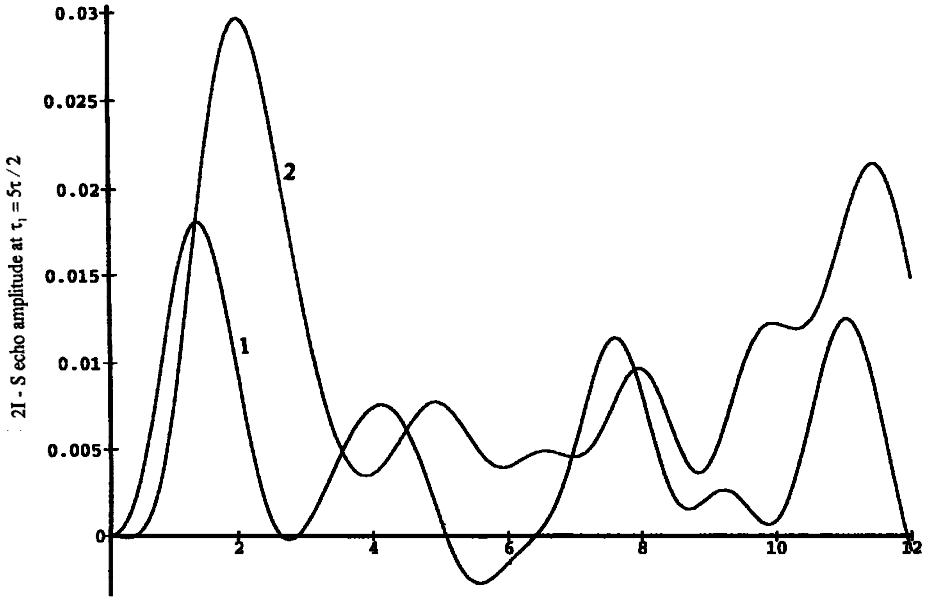

Figure 11. Spin echo amplitude $E_y^{2,3}(t_1, t_2, \tau_1 = 5\tau/2)$, $\omega_1/2\pi = 50$ kHz, as a function of the second pulse length t_2 (μs) for (1) $t_1 = 3$ μs, $\omega_Q/2\pi = 50$ kHz; (2) spin echo amplitude $E_x^{2,3}(t_1, t_2, \tau_1 = 5\tau/2)$, $\omega_1/2\pi = 50$ kHz, for $t_1 = 3$ μs, $\omega_Q/2\pi = 50$ kHz.

(11) The amplitudes of the 11th echo located at $\tau_2 = 5\tau/2$ are given by

$$E_y^{2,3}(t_1, t_2, \tau_1 = 5\tau/2) = -((I_x^{1,3} + I_x^{1,6})F_{19} - (I_x^{1,3} - I_x^{1,6})F_{20} + (I_y^{1,3} + I_y^{1,6})F_{17} + (I_y^{1,3} - I_y^{1,6})F_{18}) \quad (26)$$

and

$$E_x^{2,3}(t_1, t_2, \tau_1 = 5\tau/2) = (I_x^{1,3} + I_x^{1,6})F_{17} + (I_x^{1,3} - I_x^{1,6})F_{18} - (I_y^{1,3} + I_y^{1,6})F_{19} + (I_y^{1,3} - I_y^{1,6})F_{20}. \quad (27)$$

This echo is the result of refocusing the 2Q ($1 \leftrightarrow 3$) and 5Q ($1 \leftrightarrow 6$) coherences.

Figure 11 shows graphs of $E_x^{2,3}(t_1, t_2, \tau_1 = 5\tau/2)$ and $E_y^{2,3}(t_1, t_2, \tau_1 = 5\tau/2)$ as functions of the second pulse length.

(12) At the time $\tau_1 = 3\tau$, two overlapping echoes of different widths are detected. The amplitudes of the echo related to the 1I-S are given by

$$E_y^{3,4}(t_1, t_2, \tau_1 = 3\tau) = -((I_x^{2,4} + I_x^{2,5})K_{11} - (I_x^{2,4} - I_x^{2,5})K_{12} + (I_y^{2,4} + I_y^{2,5})K_9 + (I_y^{2,4} - I_y^{2,5})K_{10}) - ((I_x^{1,2} + I_x^{1,7})K_{15} - (I_x^{1,2} - I_x^{1,7})K_{16} + (I_y^{1,2} + I_y^{1,7})K_{13} + (I_y^{1,2} - I_y^{1,7})K_{14}) \quad (28)$$

and

$$E_x^{3,4}(t_1, t_2, \tau_1 = 3\tau) = (I_x^{2,4} + I_x^{2,5})K_9 + (I_x^{2,4} - I_x^{2,5})K_{10} - (I_y^{2,4} + I_y^{2,5})K_{11} + (I_y^{2,4} - I_y^{2,5})K_{12} + (I_x^{1,2} + I_x^{1,7})K_{13} + (I_x^{1,2} - I_x^{1,7})K_{14} - (I_y^{1,2} + I_y^{1,7})K_{15} + (I_y^{1,2} - I_y^{1,7})K_{16}. \quad (29)$$

This echo is the result of refocusing the O-S ($1 \leftrightarrow 2$), 2Q ($2 \leftrightarrow 4$), 3Q ($2 \leftrightarrow 5$) and 6Q ($1 \leftrightarrow 7$) coherences.

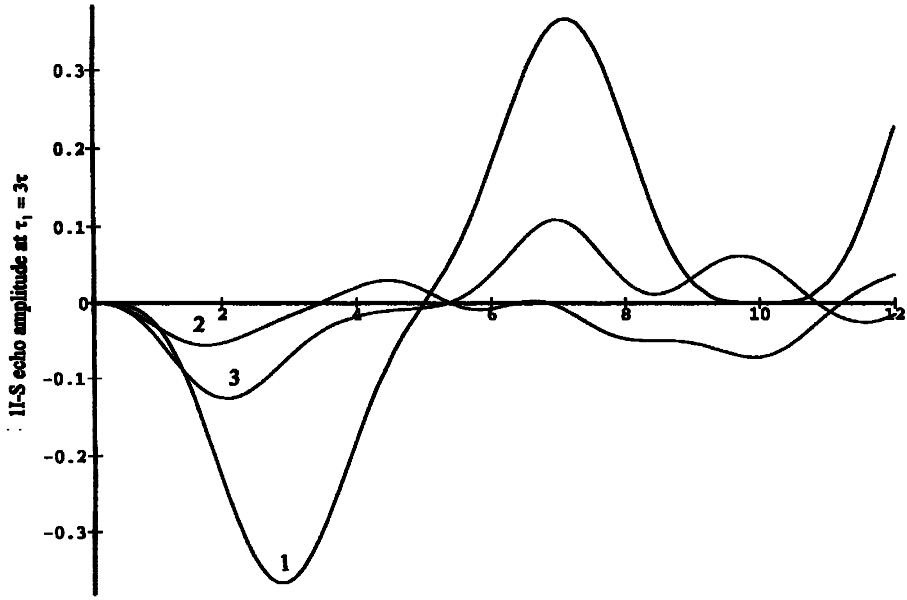

Figure 12. Spin echo amplitude $E_y^{3,4}(t_1, t_2, \tau_1 = 3\tau)$, $\omega_1/2\pi = 50$ kHz, as a function of the second pulse length t_2 (μs) for (1) $t_1 = 5$ μs, $\omega_Q/2\pi = 0$ kHz; (2) $t_1 = 3$ μs, $\omega_Q/2\pi = 50$ kHz; (3) spin echo amplitude $E_x^{3,4}(t_1, t_2, \tau_1 = 3\tau)$, $\omega_1/2\pi = 50$ kHz, for $t_1 = 3$ μs, $\omega_Q/2\pi = 50$ kHz.

Figure 12 shows graphs of $E_x^{3,4}(t_1, t_2, \tau_1 = 3\tau)$ and $E_y^{3,4}(t_1, t_2, \tau_1 = 3\tau)$ as functions of the second pulse length.

(13) The amplitudes of the echo related to the 2I-S are given by

$$E_y^{2,3}(t_1, t_2, \tau_1 = 3\tau) = -((I_x^{1,4} + I_x^{1,5})F_{23} - (I_x^{1,4} - I_x^{1,5})F_{24} + (I_y^{1,4} + I_y^{1,5})F_{21} + (I_y^{1,4} - I_y^{1,5})F_{22}) \quad (30)$$

and

$$E_x^{2,3}(t_1, t_2, \tau_1 = 3\tau) = (I_x^{1,4} + I_x^{1,5})F_{21} + (I_x^{1,4} - I_x^{1,5})F_{22} - (I_y^{1,4} + I_y^{1,5})F_{23} + (I_y^{1,4} - I_y^{1,5})F_{24}. \quad (31)$$

This echo is the result of refocusing the 3Q ($1 \leftrightarrow 4$) and 4Q ($1 \leftrightarrow 5$) coherences.

Figure 13 shows graphs of $E_x^{2,3}(t_1, t_2, \tau_1 = 3\tau)$ and $E_y^{2,3}(t_1, t_2, \tau_1 = 3\tau)$ as functions of the second pulse length.

(14) The amplitudes of the 14th echo located at $\tau_1 = 5\tau$ are given by

$$E_y^{3,4}(t_1, t_2, \tau_1 = 5\tau) = -((I_x^{1,3} + I_x^{1,6})K_{19} - (I_x^{1,3} - I_x^{1,6})K_{20} + (I_y^{1,3} + I_y^{1,6})K_{17} + (I_y^{1,3} - I_y^{1,6})K_{18}) \quad (32)$$

and

$$E_x^{3,4}(t_1, t_2, \tau_1 = 5\tau) = (I_x^{1,3} + I_x^{1,6})K_{17} + (I_x^{1,3} - I_x^{1,6})K_{18} - (I_y^{1,3} + I_y^{1,6})K_{19} + (I_y^{1,3} - I_y^{1,6})K_{20}. \quad (33)$$

This echo is the result of refocusing the 2Q ($1 \leftrightarrow 3$) and 5Q ($1 \leftrightarrow 6$) coherences.

Figure 14 shows graphs of $E_x^{3,4}(t_1, t_2, \tau_1 = 5\tau)$ and $E_y^{3,4}(t_1, t_2, \tau_1 = 5\tau)$ as functions of the second pulse length.

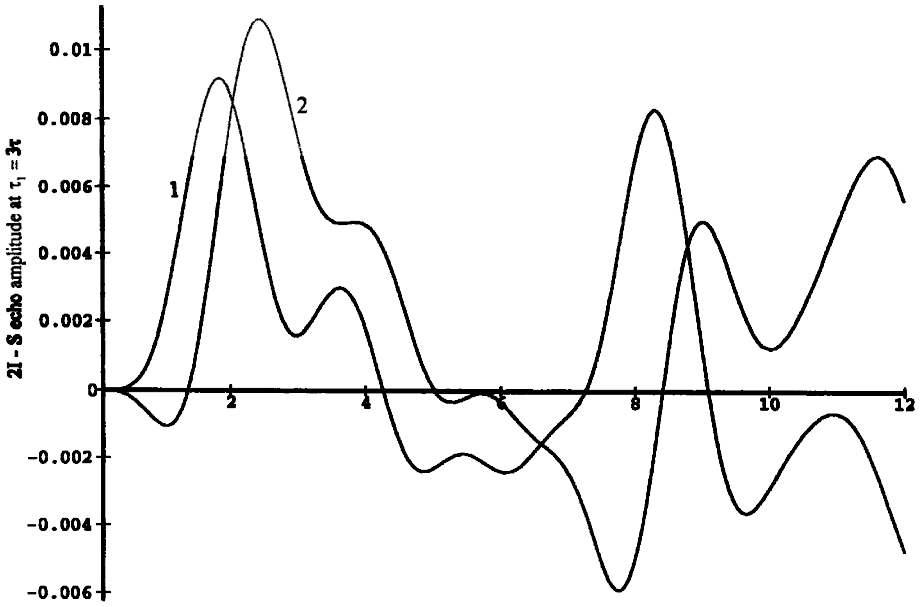

Figure 13. Spin echo amplitude $E_y^{2,3}(t_1, t_2, \tau_1 = 3\tau)$, $\omega_1/2\pi = 50$ kHz, as a function of the second pulse length t_2 (μs) for (1) $t_1 = 3$ μs, $\omega_Q/2\pi = 50$ kHz; (2) spin echo amplitude $E_x^{2,3}(t_1, t_2, \tau_1 = 3\tau)$, $\omega_1/2\pi = 50$ kHz, for $t_1 = 3$ μs, $\omega_Q/2\pi = 50$ kHz.

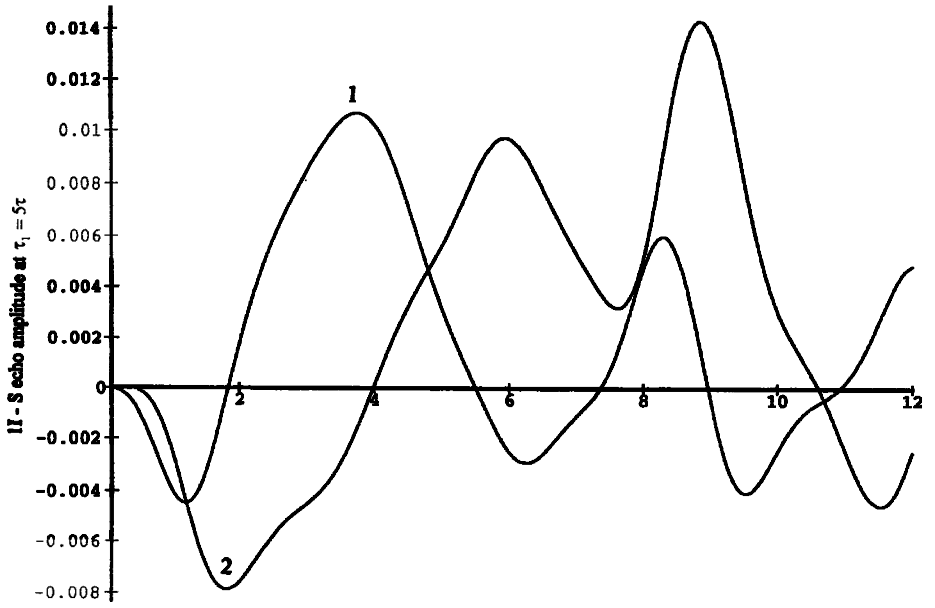

Figure 14. Spin echo amplitude $E_y^{3,4}(t_1, t_2, \tau_1 = 5\tau)$, $\omega_1/2\pi = 50$ kHz, as a function of the second pulse length t_2 (μs) for (1) $t_1 = 3$ μs, $\omega_Q/2\pi = 50$ kHz; (2) spin echo amplitude $E_x^{3,4}(t_1, t_2, \tau_1 = 5\tau)$, $\omega_1/2\pi = 50$ kHz, for $t_1 = 3$ μs, $\omega_Q/2\pi = 50$ kHz.

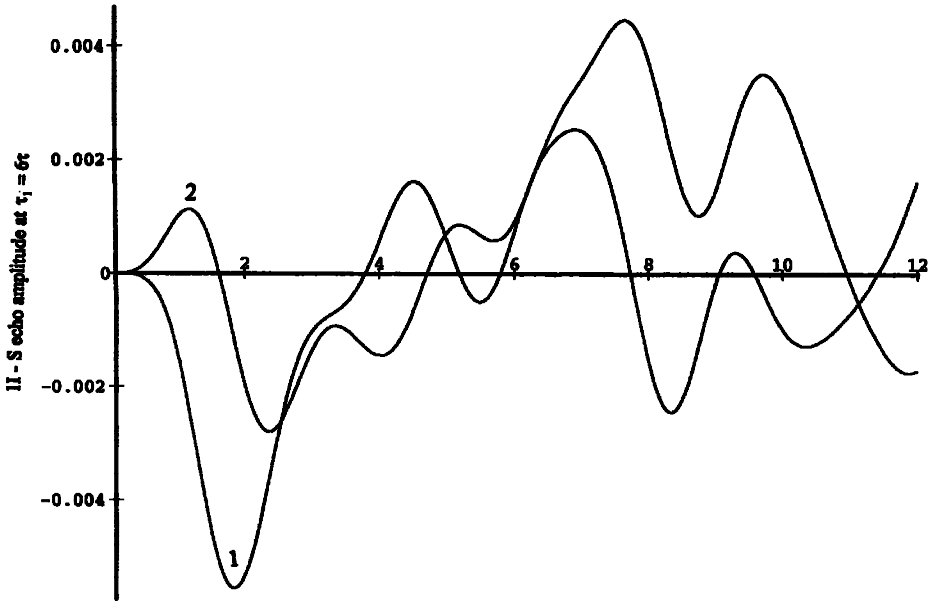

Figure 15. Spin echo amplitude $E_y^{3,4}(t_1, t_2, \tau_1 = 6\tau)$, $\omega_1/2\pi = 50$ kHz, as a function of the second pulse length t_2 (μs) for (1) $t_1 = 3$ μs, $\omega_Q/2\pi = 50$ kHz; (2) spin echo amplitude $E_x^{3,4}(t_1, t_2, \tau_1 = 6\tau)$, $\omega_1/2\pi = 50$ kHz, for $t_1 = 3$ μs, $\omega_Q/2\pi = 50$ kHz.

(15) The amplitudes of the 15th echo located at $\tau_1 = 6\tau$ are given by

$$E_y^{3,4}(t_1, t_2, \tau_1 = 6\tau) = -((I_x^{1,4} + I_x^{1,5})K_{23} - (I_x^{1,4} - I_x^{1,5})K_{24} + (I_y^{1,4} + I_y^{1,5})K_{21} + (I_y^{1,4} - I_y^{1,5})K_{22}) \quad (34)$$

and

$$E_x^{3,4}(t_1, t_2, \tau_1 = 6\tau) = (I_x^{1,4} + I_x^{1,5})K_{21} + (I_x^{1,4} - I_x^{1,5})K_{22} - (I_y^{1,4} + I_y^{1,5})K_{23} + (I_y^{1,4} - I_y^{1,5})K_{24}. \quad (35)$$

This echo is the result of refocusing the 3Q ($1 \leftrightarrow 4$) and 4Q ($1 \leftrightarrow 5$) coherences.

Figure 15 shows graphs of $E_x^{3,4}(t_1, t_2, \tau_1 = 6\tau)$ and $E_y^{3,4}(t_1, t_2, \tau_1 = 6\tau)$ as functions of the second pulse length.

The echoes discussed in 1 to 15 above are the functions of the first and second pulse lengths. In order to optimize the echo amplitudes, it is necessary to choose both pulse lengths suitably. It should be noted that figures 1–15 are plotted for the case of a single crystal only. In addition, it is seen from equations (6)–(35) that x components of the echoes are important for the medium values of ω_Q and these tend to zero when ω_Q is much greater or much less than ω_1.

It should be noted here that the six echoes at $\tau_1 = 5\tau/3, \tau_1 = 2\tau$ (O-S), $\tau_1 = 5\tau/2, \tau_1 = 3\tau$ (2I-S), $\tau_1 = 5\tau, \tau_1 = 6\tau$ are 'forbidden' in the sense that these cannot be predicted with the calculation based upon 'hard' pulse excitation. These echoes result from refocusing of exclusively multiple-quantum transitions. The expressions for the echoes for 'hard' pulse excitation are easily obtained from equations (6)–(19), (22), (23), (28) and (29) by neglecting multiple-quantum coherences and substituting $\omega_Q = 0$ in the equations for the Xs, Ys, Zs, Ts and ω_{ij}s [10]. The immediate result of these changes is that all x components of the echoes are zeroes, as expected.

4. Conclusions

Here Solomon echoes are considered for the 'soft' pulse excitation for spin 7/2. Nine echoes are predicted to arise if the pulses are 'hard'. In addition, six forbidden echoes are calculated which arise exclusively from the refocusing of multiple-quantum coherences developed during the first pulse. The amplitudes and the shapes of these echoes depend upon both pulse lengths and the ratio of ω_Q/ω_1. Our results are valid for any ratio of ω_Q/ω_1.

References

[1] Man, P. P., 1994, *Z. Naturf.*, **49a**, 89.
[2] Man, P. P., 1995, *J. magn. Reson.*, A, **114**, 59.
[3] Solomon, I., 1958, *Phys. Rev.*, **110**, 61.
[4] Hahn, E. L., 1950, *Phys. Rev.*, **80**, 580.
[5] Sanctuary, B. C., and Halstead, T. K., 1990, *Adv. magn. opt. Reson.*, **15**, 79.
[6] Bagguley, D. M. S. (editor), 1992, *Pulsed Magnetic Resonance: NMR, ESR and Optics* (Oxford: Clarendon Press).
[7] Frydman, L., and Harwood, J. S., 1995, *J. Amer. Chem. Soc.*, **117**, 5367.
[8] Ageev, S. Z., Man, P. P., Fraissard, J., and Sanctuary, B. C., 1996, *Molec. Phys.*, (submitted).
[9] Char, B. W., Geddes, K. O., Gonnet, G. H., Leong, B. L., Monagen, M. B., and Watt, S. M., 1993, *MAPLE V, Language Reference Manual: MAPLE V Library Reference Manual* (Berlin: Springer-Verlag).
[10] Ageev, S. Z., and Sanctuary, B. C., 1995, *Molec. Phys.*, **84**, 835.